



# Deactivation of titania-supported ruthenium catalysts for levulinic acid hydrogenation to gamma-valerolactone

Adarsh Patil <sup>1</sup>, Amin Delparish, Remy Creemers, John van der Schaaf, Fernanda Neira D'Angelo <sup>1,\*</sup>

<sup>1</sup> Technische Universiteit Eindhoven, Eindhoven, 5600MB, Noord Brabant, The Netherlands

## ARTICLE INFO

### Keywords:

Deactivation  
Levulinic acid  
 $\gamma$ -valerolactone  
Hydrogenation  
Kinetics

## ABSTRACT

Hydrogenation of levulinic acid (LA) to  $\gamma$ -valerolactone (GVL) is an important conversion in biomass valorization. Supported-ruthenium catalysts, typically used in aqueous phase conditions, exhibit excellent activity, albeit suffering from deactivation. This work investigates the (in)stability of Ru/TiO<sub>2</sub> during LA hydrogenation at 100–200 °C, the deactivation mechanism and kinetics. TGA and ICP analyses ruled out coking and leaching as deactivation causes. TEM and CO chemisorption show sintering of Ru particles causing low dispersion and loss of activity. However, the deactivation rate decreases with temperature, thus indicating another deactivation mechanism. Regardless, the inherent catalytic activity, expressed as TOF, remains the same. Moreover, greater Ru dispersion loss in presence of LA as compared to pure aqueous media shows that LA accelerates deactivation. Hence, increasing LA concentration leads to quicker deactivation. XPS analysis shows a reduction of Ru and Ti species (increasing Ru<sup>0</sup> and Ti<sup>3+</sup> content), alongside the decline in catalytic activity over time. After initial deactivation, both catalytic activity and oxidation state of surface species stabilize. The deactivation rate and final stable activity depend on total Ru loading, affecting spatial LA conversion and carboxylic acids concentration in the bed. Therefore, inadvertent operation with excess of Ru, either in total catalyst mass or Ru loadings on the support, and at higher temperatures (i.e., greater conversions and GVL selectivity) lead to masking of deactivation phenomena. Additional co-feeding experiments with the intermediate, 4-hydroxypentanoic acid, confirm LA as the carboxylic acid species predominantly causing deactivation. Furthermore, we study the kinetics of LA hydrogenation on the stabilized catalyst, and demonstrate that reaction kinetics transition from a zero to first-order dependence on LA from initial to stabilized activity. Additional experiments reveal a half-order dependence on hydrogen, valid from 100 to 200 °C.

## 1. Introduction

The substitution of industrial commodities derived from fossil sources by renewable counterparts is a primary focus of chemical research. To accomplish this, the efficient conversion of lignocellulosic biomass, assumed through agricultural, forestry, paper, and pulp waste, to target chemicals is recognized as a promising strategy.  $\gamma$ -valerolactone (GVL) is one of such target chemicals due to its value as a sustainable solvent and fuel additive. GVL is produced via levulinic acid (LA) hydrogenation under aqueous phase conditions or in the presence of a water-miscible organic solvent. Numerous works have reported the application of different supported-metal (Ru [1,2], Ni [3,4], Pt [5,6]) catalysts for LA hydrogenation to GVL. The recent predisposition of the catalysis community towards low temperature (<100 °C) operation for LA hydrogenation to GVL has shifted some focus towards Ru

as the active metal. An extensive list of supports and solvents have been explored for Ru catalyzed LA hydrogenation. Carbon [7–10], SiO<sub>2</sub> [1,8,11], Al<sub>2</sub>O<sub>3</sub> [8,12], TiO<sub>2</sub> [8,13,14] and zeolites [2,11,15] have been reported. Water and organic solvents such as 1,4 dioxane, isopropanol, *sec*-butylphenol have proved to be successful in this conversion. Its relative abundance and nontoxic and non-hazardous properties make water the optimal solvent. The region of interest for the reaction temperature varies from 50 to 250 °C. Although lower temperature operations present some advantages (e.g., lower preheating requirement, potentially cheaper material of construction), higher reaction temperatures enhance catalyst productivity and enable better heat recovery for exothermic processes at large scale, offsetting the limitations of higher operating temperatures [16,17].

However, Ru catalysis has recently been reported to suffer from deactivation. Abdelrahman et al. [7] reported reversible and irreversible

\* Corresponding author.

E-mail address: [m.f.neira.dangelo@tue.nl](mailto:m.f.neira.dangelo@tue.nl) (F.N. D'Angelo).

<https://doi.org/10.1016/j.cej.2025.165037>

Received 16 February 2025; Received in revised form 1 May 2025; Accepted 16 June 2025

Available online 27 June 2025

1385-8947/© 2025 The Authors. Published by Elsevier B.V. This is an open access article under the CC BY license (<http://creativecommons.org/licenses/by/4.0/>).

deactivation of commercial 5 wt% Ru/C for aqueous LA hydrogenation at 50–100 °C. Reversible deactivation was ascribed to the reversible alterations of the oxidation state of Ru upon exposure to hydrogen, while the irreversible deactivation was attributed to sintering. Additionally, loss of crystalline structure of the carbon support was observed. Further investigation by the same group using different supports in the presence of ketonic carboxylic acids revealed a negative influence of electronegativity of the supports on irreversible deactivation (i.e., sintering) [8]. Ftouni et al. [13] reported similar deactivation of Ru-based catalysts for LA hydrogenation in the presence of 1,4-dioxane as solvent. Deposition of carbonaceous species and irreversible sintering of Ru particles were reported to be the causes of deactivation.

While there is sufficient evidence of catalyst deactivation in the recent literature on LA hydrogenation, the exact deactivation mechanism and its impact on kinetics remain a subject of research. Earlier kinetic studies on this reaction focused on the use of fresh catalysts and relatively short batch reactions, where deactivation phenomena could be neglected [2,9,18,19]. Thus, understanding the nature of catalyst deactivation under aqueous LA hydrogenation and its effects on LA hydrogenation kinetics after activity stabilization (i.e., after initial deactivation) remains crucial for making an informed decision on reactor choice and operational parameters. Even more, the technical viability of Ru-based catalysts for GVL production from biomass resources can be understood from these insights. Besides this, catalytic supports exhibiting resistance to corrosive aqueous media, typically present during biomass processing, and withstanding oxidative conditions necessary for catalyst regeneration are an ideal choice. TiO<sub>2</sub> has been shown to be stable in aqueous phase at 200 °C over the entire pH range [20] and remains a widespread support choice for numerous metal-catalyzed hydrogenation reactions [21]. Therefore, in this work, the stability of TiO<sub>2</sub>-supported Ru catalysts was investigated. For the first time in literature, the effect of temperature, feed concentration, and Ru loadings on deactivation kinetics was explored. A comprehensive characterization of spent and fresh catalysts was performed to identify the causes of deactivation. This work also sheds light on the deactivation kinetics and studies the LA hydrogenation kinetics upon reaching stabilized activities.

## 2. Experimental

### 2.1. Catalyst preparation

TiO<sub>2</sub>-supported Ru catalysts were prepared using incipient wetness impregnation method. Commercially available TiO<sub>2</sub> (Degussa P-25, procured from Sigma-Aldrich) was used as the support. Typically, 1 gram of catalyst was prepared using a pre-requisite amount of RuCl<sub>3</sub>·xH<sub>2</sub>O (Sigma Aldrich, 38–40 wt% Ru) dissolved in 1.1 mL of distilled water and 0.99 g of P-25 (TiO<sub>2</sub>) nanopowder. The obtained paste was left to dry for 3 h at room temperature. The dried catalyst was pelletized and sieved to the desired particle size (53–80 µm or stated otherwise). The obtained powder was pre-reduced in a tubular oven at 450 °C for 4 h at 2 °C min<sup>-1</sup> with 5% H<sub>2</sub>/95% Ar mixture and cooled down naturally.

### 2.2. Activity testing

The required mass of catalyst was then diluted with SiC and packed in a stainless steel tubular reactor (1 cm I.D. and 10 cm length). A 10 µm and 2 µm frit with metal gaskets were used upstream and downstream of the reactor, to prevent catalyst fouling with any solids and washing away of the catalyst bed, respectively. The reactor was then leak tested at 1.25 times the operating pressure with nitrogen prior to flow experiments. LA hydrogenation was performed in an upflow packed bed reactor placed in an oven with a gas-liquid separator at the reactor outlet from where liquid samples were taken. For all catalytic runs in this work (if not mentioned otherwise), 1 mL min<sup>-1</sup> of liquid

flow rate was pumped through a Teledyne ISCO 500D syringe pump. H<sub>2</sub> flow rate of 40 N m L min<sup>-1</sup> was maintained using a Bronkhorst mass flow controller (MFC). The reactor pressure was maintained using a back-pressure controller (Bronkhorst EL-Press P-502C). Catalytic runs over a range of 100–200 °C and 21–31 bar H<sub>2</sub> pressure were performed.

### 2.3. Product analysis

Samples collected from the reactor outlet were analyzed by HPLC (Zorbax StableBond phenyl reversed phase 4.6 × 250 mm column) connected to a UV/vis detector. The eluent used was 80 vol.% 0.5 mM H<sub>2</sub>SO<sub>4</sub> in water and 20 vol.% methanol. The total eluent flow rate was 0.3 mL min<sup>-1</sup> and the oven temperature was maintained at 24 °C. The catalytic performance was studied in terms of (%) conversion of LA and (%) product yield as defined below:

$$\text{Conversion (X}_{LA}) = \frac{C_{\text{substrate, initial}} - C_{\text{substrate, reactor outlet}}}{C_{\text{substrate, initial}}} \cdot 100 \quad (1)$$

$$\text{Yield}_i = \frac{C_{\text{product, reactor outlet}}}{C_{\text{substrate, initial}}} \cdot 100 \quad (2)$$

$$\text{Selectivity}_i (S_i) = \frac{C_{\text{product, reactor outlet}}}{C_{\text{substrate, initial}} - C_{\text{substrate, reactor outlet}}} \cdot 100 \quad (3)$$

$$\text{Liquid residence time } (\tau) = \frac{V_R \cdot \epsilon_{\text{liquid}}}{Q_{\text{liquid flowrate}}} \quad (4)$$

where  $\epsilon_{\text{liquid}}$  is the liquid hold-up. Void fraction for solid is assumed to be 0.6 for a typical packed bed reactor.

$$\text{Catalytic activity } (a) = \frac{(C_{LA, \text{initial}} - C_{LA, \text{reactor outlet}}) \cdot Q_{\text{flowrate}}}{W_{Ru}} \quad (5)$$

where  $W_{Ru}$  is the mass of Ru loading in the catalytic bed in grams.

Calibrations for levulinic acid (LA, 98%, Sigma Aldrich) and  $\gamma$ -valerolactone (GVL, 98%, Sigma Aldrich) were performed using the peak response at  $\lambda = 205$  nm using the UV-Vis detector. Since 4-hydroxy pentanoic acid (4-HPA) was unavailable, its sodium salt, sodium 4-hydroxypentanoate (CAS no. 56279-37-9), was procured from Merck Life Sciences (Article no. BL3H97A45B64-250MG) and protonated to 4-HPA using 5 mM H<sub>2</sub>SO<sub>4</sub> at room temperature, followed by calibration. **NOTE:** Other HPLC columns and their effects of 4-HPA selectivity with further implications on data interpretation are discussed in Appendix G in SI.

### 2.4. Catalyst characterization

X-ray photoelectron spectroscopy (XPS) was performed on the spent samples to find the oxidation state of Ru using a Thermo Scientific K-Alpha XPS system with a 180° double-focusing hemispherical analyser with a 128-channel detector. The X-ray source was an Al K $\alpha = 1486.68$  eV micro-focused monochromator with a spot size of 400 µm.

Transmission electron microscopy (TEM) was used to determine the Ru particle size. TEM samples were prepared by crushing the catalysts followed by suspending in ethanol. The samples were analyzed by a FEI Tecnai G2 Sphera cryo TEM operated at 200 kV. The TEM micrographs were processed using ImageJ to find the Ru particle size of at least 150 particles per sample.

Thermogravimetric analysis (TGA) was performed on the spent samples to detect strongly adsorbed components using a TA-instruments TGA 550. Measurements were performed using 10 to 15 mg samples in air and at atmospheric pressure. The initial ramp was 10 °C min<sup>-1</sup> to 100 °C, the samples were then stabilized for 10 min and the final ramp was 10 °C min<sup>-1</sup> to 750 °C.

X-ray powder diffraction (XRD) patterns were obtained by a Rigaku MiniFlex 600 diffractometer with Cu-K $\alpha$  (0.154 nm) source and equipped with a K $\beta$  (x2) filter with constant step of 0.02° 2 $\theta$  and counting time of 2 s per step. Intensity at angles between 10–90° was measured at a rate of 0.6° min<sup>-1</sup>.

CO chemisorption was performed on the fresh and spent samples to determine Ru dispersion using Micromeritics AutoChem III. For a typical CO chemisorption experiment, the samples were first pre-treated in He at 150 °C. In case of fresh samples, the temperature was cooled down to 50 °C and the samples were then reduced in 10% H<sub>2</sub> in Ar at 450 °C for 4 h at 2° min<sup>-1</sup>. The samples were then cooled down to 50 °C, subsequently followed by CO pulse chemisorption at 50 °C until similar peak area was attained.

## 2.5. Deactivation kinetics fitting

Catalytic activity ( $a$ ), expressed in  $\text{mol}_{\text{LA,conv.}} \cdot \text{g}_{\text{Ru}}^{-1} \cdot \text{h}^{-1}$ , was calculated according to Eq. (5). Deactivation kinetics [22] were modeled, as being first order with respect to catalytic activity at a given time, using the equations stated below:

$$-\frac{da}{dt} = k_{\text{deactivation}} \cdot (a^n - a_{\infty}) \quad (6)$$

Substituting  $n = 1$ ,  $a$  can be expressed as

$$a = (a_0 - a_{\infty}) \cdot e^{-k_{\text{deactivation}} \cdot t} + a_{\infty} \quad (7)$$

wherein,  $t$  is time on stream in hours,  $k_{\text{deactivation}}$  is the deactivation constant in  $\text{h}^{-1}$  and  $a_{\infty}$  is the stabilized activity in  $\text{mol}_{\text{LA,conv.}} \cdot \text{g}_{\text{Ru}}^{-1} \cdot \text{h}^{-1}$ . Furthermore, the deactivation constant can be expressed as a function of temperature via Arrhenius dependence as shown below [22]

$$k_{\text{deactivation}} = k_{\text{deactivation},0} \cdot e^{-H_{\text{deactivation}}/RT} \quad (8)$$

wherein  $H_{\text{deactivation}}$  is analogous to Arrhenius energy, expressed in  $\text{kJ mol}^{-1}$ . The obtained experimental values were then fitted to an error objective function that was defined as the sum of the root mean square errors (RMSE) between the experimental and calculated catalytic activity as follows:

$$\text{RMSE} = \sqrt{\frac{\sum_{k=1}^{N_{\text{data}}} (y_k^{\text{calc}} - y_k^{\text{exp}})^2}{N_{\text{data}}}} \quad (9)$$

where  $N_{\text{data}}$  is the number of experimental data used for kinetic fitting and  $y_k^{\text{calc}}$  and  $y_k^{\text{exp}}$  are catalytic activities determined via the model fitting and experimentally, respectively. The error objective function was minimized using the built-in *lsqnonlin* function in MATLAB 2023.

## 3. Results

### 3.1. Catalyst screening

Several supports such as TiO<sub>2</sub> [8,13,14], ZrO<sub>2</sub> [13], carbon [7–10], SiO<sub>2</sub> [8,11] and zeolites [2,11,15] have been reported for LA hydrogenation. A comprehensive summary of these is shown in Table 1. Based on their reported performance, three supports, i.e., ZrO<sub>2</sub>, TiO<sub>2</sub>, and USY-zeolite were chosen in our screening experiments (See Fig. 1). Near complete conversion of LA was observed with Ru/TiO<sub>2</sub>, while only 60% of LA was converted with Ru/USY-zeolite. The selectivity to GVL remained ~95% in both cases. Ru/ZrO<sub>2</sub> was unable to achieve any perceptible conversion under the present conditions, although previous studies have reported better activities in 1,4-dioxane as a solvent [13]. Thus, Ru/TiO<sub>2</sub> was chosen for further investigation in this work.

Table 1 shows LA hydrogenation data for various catalysts and conditions. Entries 1 to 10 have employed a continuous flow-through reactor configuration while the following entries are reported using batch reactors. In general, it is evident that the GVL productivity achieved with batch reactor is significantly higher than the flow counterparts. This is predominantly due to the remarkably longer liquid residence time used in batch. These conditions render high GVL yields ( $\geq 95\%$ ) despite a relatively lower catalyst loading. Several works have demonstrated that LA hydrogenation to GVL occurs via rapid formation of 4-hydroxypentanoic acid (4-HPA) as intermediate, followed by the relatively slower 4-HPA ring closure to GVL. This second step can also

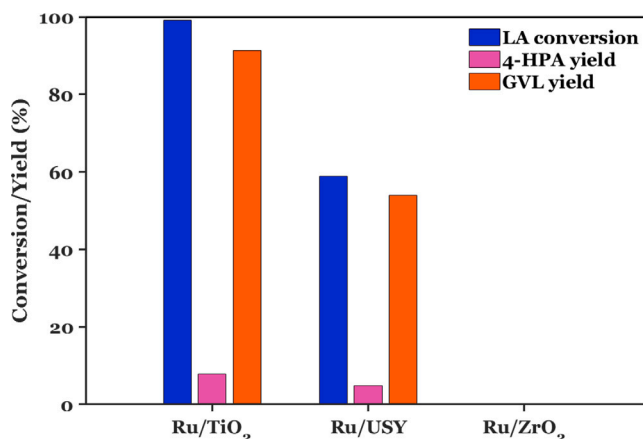


Fig. 1. Different support screening for LA hydrogenation to GVL using 1 wt% Ru as active metal catalyst. Reaction conditions:  $T = 200^\circ \text{C}$ ;  $P_{\text{H}_2} = 31 \text{ bar}$ ;  $C_{\text{LA}} = 2 \text{ wt\%}$ ;  $W_{\text{cat}} = 0.2 \text{ g}$ ;  $W_{\text{SiC}} = 3.8 \text{ g}$ ;  $Q_{\text{feed}} = 1 \text{ mL min}^{-1}$ ;  $Q_{\text{H}_2} = 40 \text{ N m L min}^{-1}$ ;  $\text{WHSV} = 300 \text{ g}_{\text{feed}} \cdot \text{g}_{\text{cat}}^{-1} \cdot \text{h}^{-1}$ . NOTE: The values reported are averaged for samples in the initial three hours of testing and no deactivation was observed.

be catalyzed homogeneously [1,9,18], so long liquid residence time and low catalyst loadings used in batch reactors render high yields and relatively large productivity per mass of catalyst. On the other hand, the flow counterparts feature higher catalyst loading per reactor volume, shorter liquid residence times, and therefore tend to be inefficient in completing the ring closure reaction, thus rendering relatively lower GVL selectivity/yields.

Alternatively to prolonging the liquid residence times, operating at higher temperatures is also effective in boosting GVL production without sacrificing carbon balance. GVL selectivity's up to ~80% are recorded in flow reactors, with 4-HPA selectivity accounting for the remaining 20%. For all the experiments performed in this work, carbon balance including unconverted LA, 4-HPA and GVL, remains  $\sim 100 \pm 2\%$ . Therefore, the formation of valeric acid from GVL [23,24], if occurring in trace amounts, can be neglected. Also, no severe formation of carbon deposits are expected under these conditions. Entries 1–3 in Table 1 correspond to data obtained in this work. The results demonstrate that high GVL selectivity and productivity can indeed be achieved with liquid residence time  $< 1 \text{ min}$  at  $200^\circ \text{C}$ . Entries 4–7 report literature data obtained with flow reactors at lower temperatures (in a similar range as those in batch studies), yielding less GVL. Additionally, in case of flow studies, GVL selectivity seems to increase with temperature, thus indicating higher activation energy of the second step, i.e., 4-HPA ring closure to GVL. Furthermore, Hommes et al. [18] and Mani et al. [1] have demonstrated the autocatalytic nature of the second step (see Appendix G in SI for a more detailed discussion). Further into the effect of temperature on product distribution using Ru/TiO<sub>2</sub> as the catalyst of choice is covered in the following sections.

### 3.2. Deactivation tests

#### Temperature effects on deactivation rates

Following evidences catalyst of deactivation [7,8,13,14], we investigate the stability of Ru/TiO<sub>2</sub> during LA hydrogenation in the temperature range  $100\text{--}200^\circ \text{C}$  over a period of five hours. To ensure incomplete conversion, the catalyst mass was halved with respect to previous experiments, i.e., from 200 to 100 mg of 1 wt% Ru/TiO<sub>2</sub>. Fig. 2 shows a clear decay in catalytic activity at all temperatures. As expected, catalytic activity at the beginning of operation is the highest for  $200^\circ \text{C}$ , and decreases with temperature due to its Arrhenius behavior. Upon several hours of time on stream, the activity reaches a plateau, hereby referred as stabilized activity. Notably, the stabilized activity at different temperatures do not differ significantly, as seen

**Table 1**  
Comparison of different Ru based catalysts reported for continuous LA hydrogenation to GVL.

Entry	Catalyst	Solvent	P (bar)	T (°C)	WHSV ( $\text{g}_{\text{feed}}^{-1} \text{g}_{\text{cat}}^{-1} \text{h}^{-1}$ )	$\tau_{\text{liq}}$ (min)	$X_{\text{LA}}$ (%)	$S_{\text{GVL}}$ (%)	TOS (h)	Prod. ( $\text{g}_{\text{GVL}}^{-1} \text{g}_{\text{cat}}^{-1} \text{h}^{-1}$ )	Ref.
1	1 wt% Ru/TiO <sub>2</sub>	H <sub>2</sub> O	31	200	300	0.54	100	95	3	4.92	This work
2	1 wt% Ru/TiO <sub>2</sub>	H <sub>2</sub> O	31	200	300	0.54	53	95	120	2.60 <sup>a,b</sup>	This work
3	2 wt% Ru/TiO <sub>2</sub>	H <sub>2</sub> O	31	200	600	0.54	50	90	140	5.82 <sup>a</sup>	This work
4	0.5 wt% Ru/C	1,4 DO <sup>1</sup>	12	130	3	4.21	100	84	1–2	0.11	[18]
5	0.5 wt% Ru/C	H <sub>2</sub> O	45	90	60	2.09	92	78	52	3.71	[10]
6	5 wt% Ru/C	H <sub>2</sub> O	41	50	550	1.10	2	3	70	0.02	[7]
7	2.5 wt% Ru/SBA-15	H <sub>2</sub> O	10	90	7.5	8–13 <sup>d</sup>	100	36	20	0.12	[1]
8	2.5 wt% Ru/SBA-15 <sup>f</sup>	H <sub>2</sub> O	10	100	4.5	8–13 <sup>d</sup>	100	86	300	0.17	[1]
9	5 wt% Ru/C	SBP <sup>2</sup>	35	180	3.6	N.A.	N.A.	N.A.	300	2.73	[25]
10	5 wt% (Ru <sub>18</sub> Sn <sub>5</sub> /C)	SBP <sup>2</sup>	35	180	1.2	N.A.	N.A.	N.A.	300	0.83	[25]
11	1 wt% Ru/TiO <sub>2</sub> <sup>e</sup>	1,4 DO <sup>1</sup>	30	150	167	180	100	98	15	14.11 <sup>c</sup>	[13]
12	1 wt% Ru/TiO <sub>2</sub> <sup>e</sup>	1,4 DO <sup>1</sup>	30	150	167	180	100	100	3	14.40	[13]
13	5 wt% Ru/C <sup>e</sup>	1,4 DO <sup>1</sup>	30	100	21	180	100	97	3	1.76	[13]
14	5 wt% Ru/C <sup>e</sup>	1,4 DO <sup>1</sup>	30	150	167	180	100	97	3	13.97	[13]
15	3 wt% Ru/C <sup>e</sup>	H <sub>2</sub> O	45	130	550	60	97	88	1	46.00	[9]
16	5 wt% Ru/C <sup>e</sup>	IPA <sup>3</sup>	N.A.	140	663	30	43	95	1	12.19 <sup>d</sup>	[26]

1 - 1,4 dioxane; 2 - *sec*-butylphenol; 3 - Isopropanol; 4 - Residence times retrieved from the work as is due to insufficient data regarding catalyst mass used.

<sup>a</sup> Values reported after achieving activity stabilization.

<sup>b</sup> Based on 200 mg catalyst loading.

<sup>c</sup> Five cycles with three hours of reaction time.

<sup>d</sup> Two cycles of 30 min of reaction time.

<sup>e</sup> Entries 11–16 are based on batch reactor studies.

<sup>f</sup> 2.5 wt% Ru/20%Nb/ SBA-15.

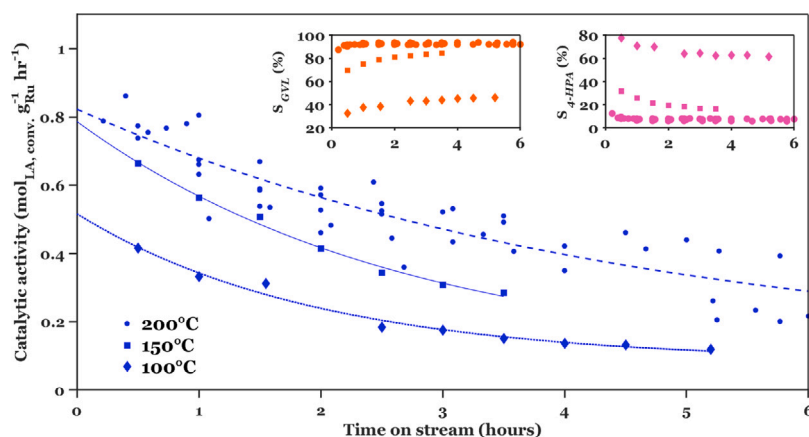


**Fig. 2.** Catalyst activity profiles vs. time at different temperatures using 1 wt% Ru/TiO<sub>2</sub> for aqueous phase LA hydrogenation. Reaction conditions:  $T = 100, 150$  and  $200^\circ\text{C}$ ;  $P_{\text{H}_2} = 31$  bar;  $C_{\text{LA}} = 2$  wt%;  $W_{\text{cat}} = 0.1$  g;  $W_{\text{SiC}} = 3.9$  g;  $Q_{\text{feed}} = 1$  mL min<sup>-1</sup>;  $Q_{\text{H}_2} = 40$  N mL min<sup>-1</sup>;  $\text{WHSV} = 600 \text{ g}_{\text{feed}}^{-1} \text{g}_{\text{cat}}^{-1} \text{h}^{-1}$ .

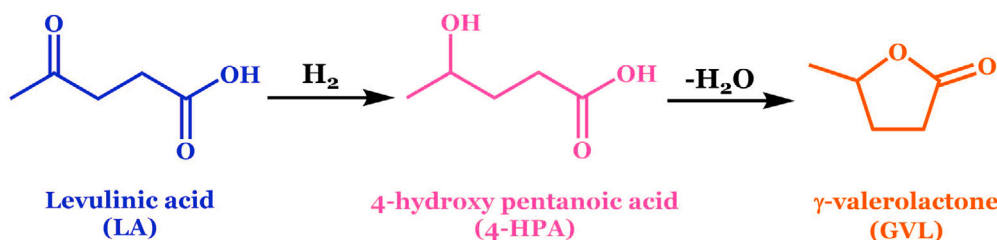


**Fig. 3.** Preferred reaction pathway of LA hydrogenation to GVL through the formation of intermediate, 4-hydroxy pentanoic acid (4-HPA).

from the raw experimental data as well as the fitting parameter, i.e.,  $a_\infty$  (see Table 2, entries 1 to 3). Further discussion on the LA hydrogenation kinetics after activity stabilization is done in Section 3.4. With respect to the rate of deactivation, it is evident that the decay in activity is fastest for the lowest temperature explored ( $100^\circ\text{C}$ ), and it decreases at greater temperature. This is unexpected if sintering is assumed as the main cause of deactivation. This evidence suggests strong adsorption of chemical species as a contributor to the activity loss.

With respect to selectivity trends, the hydrogenation of LA under the present conditions leads to two main products, namely 4-HPA and GVL, formed according to scheme Fig. 3. This is the generally accepted pathway, instead of the rearrangement of LA to form  $\alpha$ -angelica lactone followed by hydrogenation to GVL [7,9,27]. As previously established, higher temperatures favor the selectivity of GVL, in agreement with several studies in the literature that demonstrate a higher activation energy for the second reaction step [7,9].



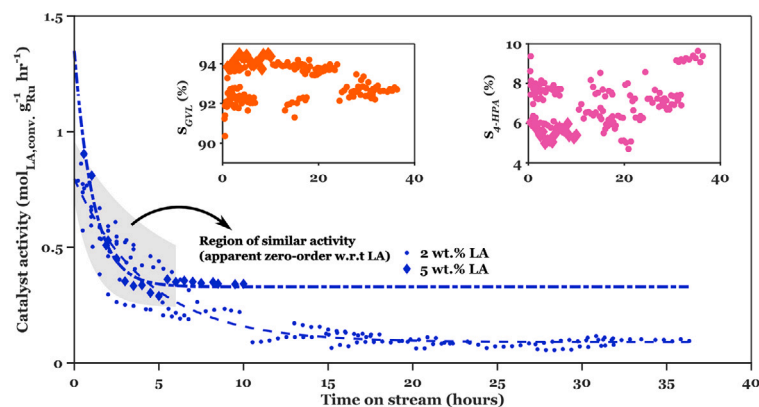


**Fig. 4.** Catalyst activity profiles vs. time using 1 wt% Ru/TiO<sub>2</sub> for aqueous phase LA hydrogenation using different LA concentrations in the feed. Reaction conditions:  $T = 200\text{ }^{\circ}\text{C}$ ;  $P_{\text{H}_2} = 31\text{ bar}$ ;  $C_{\text{LA}} = 2$  and 5 wt%;  $W_{\text{cat}} = 0.1\text{ g}$ ;  $W_{\text{SiC}} = 3.9\text{ g}$ ;  $Q_{\text{feed}} = 1\text{ mL min}^{-1}$ ;  $Q_{\text{H}_2} = 40\text{ N m L min}^{-1}$ ;  $\text{WHSV} = 600\text{ g}_{\text{feed}}^{-1}\text{ g}_{\text{cat}}^{-1}\text{ h}^{-1}$ . Diamond markers indicate results for 5 wt% LA.

Besides, a discernible shift in product distribution is observed upon time on stream. Under all temperatures explored, the selectivity to the final product, GVL, in fact increases upon deactivation. We hypothesize that the changes in catalytic activity during operation selectively inhibit the first reaction step (i.e., the metal-catalyzed hydrogenation of LA to 4-HPA), leaving the second step (i.e. the partly homogeneously acid-catalyzed ring closure of 4-HPA to GVL) relatively unaffected. The results indicate that the conversion of 4-HPA to GVL at  $200\text{ }^{\circ}\text{C}$ , even on deactivated catalyst, is rather fast. Based on the above, we hypothesize that relatively large concentrations of LA or 4-HPA (i.e., typically found at lower temperatures and short times) are conducive to faster deactivation. Presumably, carboxylic acid groups introduce competitive adsorption on the active sites, and therefore cause a reduction of LA hydrogenation rate.

#### Concentration effects on deactivation rates

To test the hypothesis of deactivation induced by presence of carboxylic acid, we study the effect of LA feed concentration on hydrogenation and deactivation rates. Fig. 4 shows catalytic activity during several hours of time on stream using 2 and 5 wt% LA as feed at  $200\text{ }^{\circ}\text{C}$ . Regardless of LA concentration, a steep decline in catalytic activity is noted in the initial hours of operation, with an evident plateau after ca. 5 and 15 h, for 5 and 2 wt% LA, respectively. Deactivation rate is faster for the more concentrated feed. The activity halves (i.e. from  $9 \cdot 10^{-4}$  to  $4.5 \cdot 10^{-4}\text{ mol}_{\text{LA,conv.}}\text{ g}_{\text{Ru}}^{-1}\text{ h}^{-1}$ ) in 2 h with 5 wt% LA, and in 5 h with 5 wt% LA for otherwise identical reaction conditions. Yet, the experiments under more dilute conditions reach a greater extent of deactivation, with final stabilized activity values proportional to LA feed concentration. On the other hand, it is interesting to note that the catalytic activity expressed in  $\text{mol}_{\text{LA,conv.}}\text{ g}_{\text{Ru}}^{-1}\text{ h}^{-1}$  during the initial hours of operation (see the gray-colored region in Fig. 4) appears to be independent of feed concentration. This suggests a pseudo zero-order kinetics of LA hydrogenation with respect to LA concentration in this region (note that the activity data during the initial hours of operation is based on integral conditions, with  $X_{\text{LA}} > 10\%$ ). Additional data with an intermediate LA concentration (i.e., 3.5 wt% LA), perfectly aligns with these trends (i.e., quicker deactivation and stabilized activity approximately 1.6 times higher those observed with 2 wt% LA feed, see Figure S17 in SI and entries 3 to 5 in Table 2). Finally, a remarkable feature of operating at  $200\text{ }^{\circ}\text{C}$  remains the relatively unchanged product distribution, with  $>90\%$  GVL selectivity, and nearly independent of LA concentrations.

#### Loading effects on deactivation kinetics

In this section, we investigate the effect of total Ru loadings through a series of experiments varying the catalyst bed. Initially, the total mass of catalyst was doubled from 100 to 200 mg while maintaining 1 wt%

Ru loading. Then, Ru loading per mass of catalyst was doubled from 1 to 2 wt% while using 100 mg of total catalyst mass. All these catalyst beds were operated at  $200\text{ }^{\circ}\text{C}$ .

Fig. 5 shows the catalytic activity as a function of TOS for the aforementioned catalyst beds. Subfigure (A) compares the performance of two catalytic beds with the exact same Ru content, each of them achieved by distinct Ru loading per gram catalyst and a correspondingly different catalyst mass. Thus, it can be easily inferred that the TiO<sub>2</sub> content was not the same in these two catalytic beds. It can be observed that the initial and stabilized activities, as well as the deactivation kinetic constants, remain nearly the same for catalyst beds (see Table 2). Therefore, the LA hydrogenation activity seems to correlate to the total Ru content, while it appears to be independent of the TiO<sub>2</sub> content in the catalyst bed at  $200\text{ }^{\circ}\text{C}$ . The loading of Ru per gram catalyst appears to be irrelevant. With respect to deactivation kinetics, both catalytic beds lose  $\sim 4\%$ – $6\%$  of their activity per hour of TOS. Finney et al. [28] have reported accelerated activity loss due to sintering while using slightly higher (i.e., 3.5 wt%) metal loadings for Pd/Al<sub>2</sub>O<sub>3</sub>, and found the same to be applicable for other noble metals including Pt, Pd, Ru, Ir, Au, and Ag. While sintering cannot be ruled out as a cause of deactivation, especially considering the high partial pressure of water and the acidic environment (i.e. conditions conducive to sintering, even at  $30\text{--}50\text{ }^{\circ}\text{C}$  [29]), the independence of deactivation rate on Ru loadings may suggest otherwise. Sintering rates usually scale with metal loadings [30].

Next, Fig. 5-B compares the effect of doubling the mass of total Ru loading, this time by doubling the total mass of the same catalyst (1 wt% Ru/TiO<sub>2</sub>), on LA hydrogenation activity normalized per gram Ru. At first sight, the divergence in these trends appears to contradict the previous observations (i.e., LA hydrogenation activity scales with total Ru loading). Nevertheless, Figure S12-(b) in SI further reveals that  $X_{\text{LA}}$  was greater than 90% during the initial phase of operation (up to TOS of 1 h), for all catalytic beds. This explains that the initial catalytic activity (based on nearly full conversion) normalized per mass Ru, as shown in Fig. 5-B, is halved on doubling Ru loading. Given the high conversion, there was likely an excess of catalysts in these initial phases of operation, preventing an accurate interpretation of the intrinsic activity and deactivation kinetics in the initial ca. 5 h. Upon increasing TOS beyond 5 h,  $X_{\text{LA}}$  decreases below  $<90\%$ , thereby allowing a more quantitative interpretation of the activity and its decay. It is evident that the catalytic bed with greater Ru loadings suffers from significantly slower deactivation. The smallest catalytic bed (i.e., 100 mg of 1 wt% Ru) suffers an activity drops of 90% while the largest bed deactivates by only 10% within 10 h of TOS. Remarkably,  $X_{\text{LA}}$  remains rather stable during the same period for higher Ru loadings (Figure S12-(b)). Eventually, when comparing the final stabilized activities, we

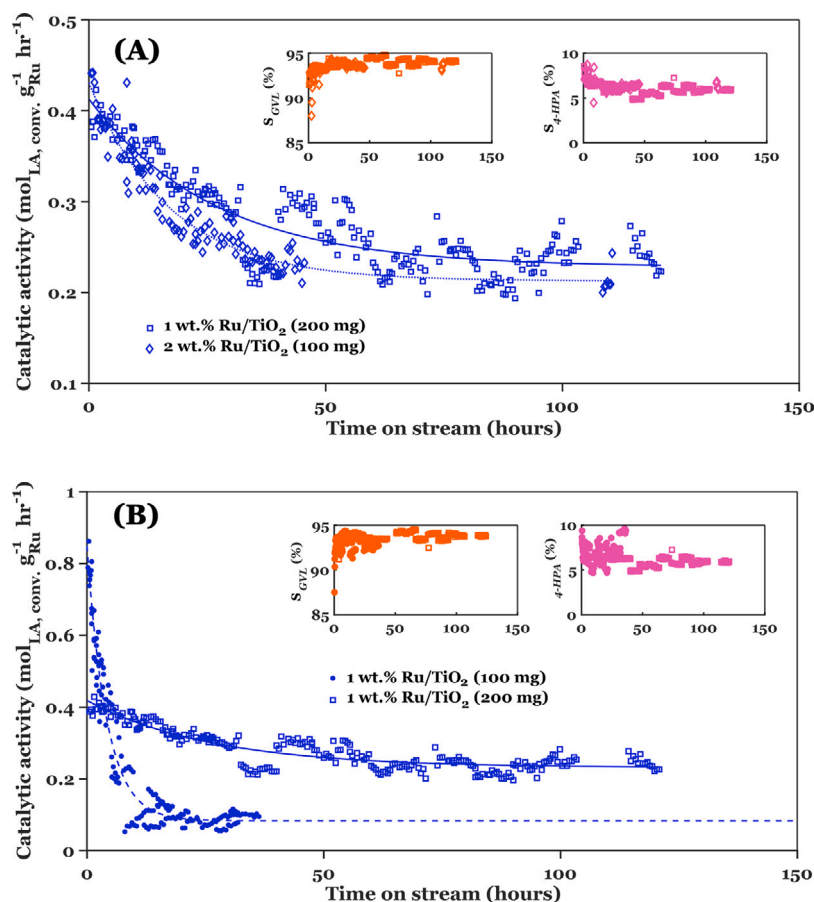


Fig. 5. Catalyst activity profiles vs. time using different Ru and catalyst loadings for aqueous phase LA hydrogenation using. Reaction conditions:  $T = 200\text{ }^{\circ}\text{C}$ ;  $P_{\text{H}_2} = 31\text{ bar}$ ;  $C_{\text{LA}} = 2\text{ wt\%}$ ;  $W_{\text{cat}}$  = mentioned in the figure;  $W_{\text{SiC}} = 3.8/3.9\text{ g}$  (based on 4 g of total packing);  $Q_{\text{feed}} = 1\text{ mL min}^{-1}$ ;  $Q_{\text{H}_2} = 40\text{ N m L min}^{-1}$ ;  $\text{WHSV} = 300/600\text{ g}_{\text{feed}}^{-1}\text{ h}^{-1}$  (based on catalyst mass used).

encounter that the Ru normalized activity is not the same for these two catalyst beds.

A plausible explanation for the slower deactivation rate at higher Ru loadings can be found in the linear dependence of deactivation rate with LA concentration earlier discussed. If we envision the 200 mg bed as two sequential halves of 100 mg catalyst each, with the first rendering nearly full conversion of LA to GVL with ca. >95% selectivity (Fig. 2 at  $200\text{ }^{\circ}\text{C}$ ), it can be inferred that the second half remains nearly free of carboxylic acids. These conditions are conducive to greater stability of the second bed, as shown in Fig. 6-B. However, upon deactivation of the first bed, lowering LA conversions below 100% will gradually increase concentrations of carboxylic acids downstream. Hence, apparent deactivation of the entire 200 mg bed occurs at a lower rate. Therefore, we hypothesize that low concentrations of carboxylic acids under these conditions is key to preserving activity. Thus, unifying the increase in catalyst loading with a more severe operating temperature consolidates the deceleration of deactivation kinetics significantly for Ru-catalyzed LA hydrogenation in aqueous conditions. Regardless, 4-HPA selectivity remains relatively unchanged,  $\sim 6\text{--}8\%$ , at  $200\text{ }^{\circ}\text{C}$ , in agreement with the previous observations for lower catalyst loadings. Furthermore, the carbon balance remains  $100 \pm 2\%$  for all scenarios at  $200\text{ }^{\circ}\text{C}$ .

While the above hypothesis may (at least qualitatively) explain the differences in deactivation rate in these two beds, the fact that the final stabilized activity  $a_{\infty}$  normalized per Ru is also different (i.e., doubling the total Ru loading renders ca. 2.5-fold increase in stabilized activity, from  $0.09$  to  $0.24\text{ mol}_{\text{LA,conv.}}\text{ g}_{\text{Ru}}^{-1}\text{ h}^{-1}$ ), deserves some consideration. After establishing that the stabilized activity scales with Ru loading (Fig. 5), and assuming zeroth order kinetics for LA hydrogenation with respect to LA, as suggested in numerous works [7,9,18],  $a_{\infty}$  should

remain relatively unchanged in this two experiments. The fact that this does not hold true suggests a change in the final catalyst structure (i.e., the intrinsic activity of these catalysts is not comparable), and/or a change in the kinetic regime towards a positive order on LA, upon reaching activity stabilization. The latter is in line with the observed effects on LA concentration on stabilized activity (Fig. 6-B).

#### Deactivation kinetics using 1 wt% Ru/TiO<sub>2</sub>

Fig. 6 shows fitted kinetic parameters for the catalyst deactivation rate (A and B) and well as the initial and stabilized catalytic activity as function of LA feed concentration (C and D). Deactivation rate decreases with temperature, as shown earlier, with an estimated activation energy of  $-12.2\text{ kJ mol}^{-1}$  (see Section 2.5). This figure is similar to the heat of adsorption ( $\Delta H_{\text{adsorption}}$ ) of LA obtained on different clays and polymeric adsorbents [31,32]. Furthermore, Fig. 6-B shows an almost linear relationship between  $k_{\text{deactivation}}$  and LA feed concentration at  $200\text{ }^{\circ}\text{C}$ . Thus, all this evidence hints towards substrate-induced (i.e., LA or 4-HPA) deactivation, very likely arising from the carboxylate species. This aligns with evidence presented by Liu et al. [14], albeit using 1,4 dioxane as the solvent, and by Abdelrehman et al. who demonstrated that the presence of carboxylic acids on Ru-supported catalysts caused significant deactivation depending on the positive surface charge of the support [8]. Drawing on these findings, the deactivation kinetic term can be expressed as follows.

$$k_{\text{deactivation}} = k_{d0} \exp(-H_{\text{deactivation}}/RT) \quad (10)$$

wherein  $k_{d0}$  and  $H_{\text{deactivation}}$  are pseudo pre-exponential factor and deactivation energy, respectively. Looking at the evidences,  $k_{d0}$  linearly depends on feed concentration as shown in Fig. 6-B, while  $H_{\text{deactivation}}$  is

**Table 2**

Deactivation kinetics fitting parameters for different temperatures, LA feed concentration, Ru and catalyst loadings for LA hydrogenation to GVL with 95% confidence intervals. Reaction conditions:  $P_{H_2} = 31$  bar;  $Q_{feed} = 1$  mL min<sup>-1</sup>;  $Q_{H_2} = 40$  N mL min<sup>-1</sup>.

Entry	T (°C)	$C_{LA}$ in H <sub>2</sub> O (wt.%)	Ru load. (wt.%)	Mass <sup>c</sup> (mg)	$a_0$ (mol <sub>LA,conv.</sub> g <sub>Ru</sub> <sup>-1</sup> h <sup>-1</sup> )	$k_{deactivation}$ (h <sup>-1</sup> )	$a_{\infty}$ (mol <sub>LA,conv.</sub> g <sub>Ru</sub> <sup>-1</sup> h <sup>-1</sup> )
1	100	2	1	100	$0.52 \pm 0.056$	$0.51 \pm 0.072$	$0.083 \pm 0.014$
2	150	2	1	100	$0.78 \pm 0.061$	$0.37 \pm 0.053$	$0.085 \pm 0.020$
3	200	2	1	100	$0.86 \pm 0.065$	$0.25 \pm 0.048$	$0.093 \pm 0.025$
4	200	3.5	1	100	$0.75 \pm 0.067$	$0.53 \pm 0.048$	$0.15 \pm 0.021$
5	200	5	1	100	$1.35 \pm 0.20$	$0.89 \pm 0.190$	$0.33 \pm 0.020$
6	200	2	1	200	$0.42 \pm 0.014$	$0.038 \pm 0.006$	$0.23 \pm 0.015$
7	200	2	2	100	$0.43 \pm 0.012$	$0.058 \pm 0.008$	$0.22 \pm 0.020$
8	100 <sup>a</sup>	2	1	100	$0.54 \pm 0.078$	$0.79 \pm 0.10$	$0.10 \pm 0.018$
9	200 <sup>b</sup>	2	1	200	$0.84 \pm 0.067$	$0.78 \pm 0.088$	$0.062 \pm 0.009$

<sup>a</sup>  $P_{H_2} = 44$  bar.

<sup>b</sup> Rutile TiO<sub>2</sub>.

<sup>c</sup> Mass of catalytic bed.

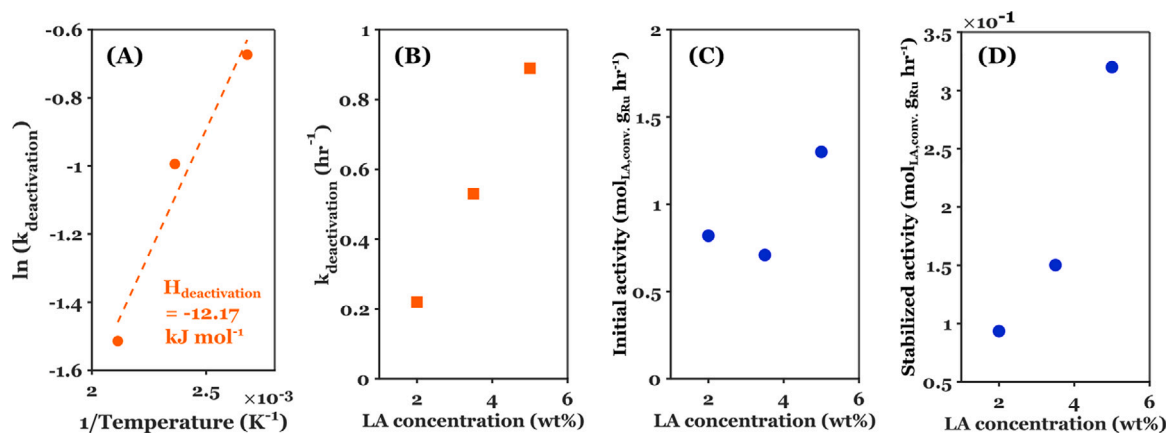
shown in subfigure A of the same. Similar expressions for reactions such as catalytic cracking [33] and ethanol dehydration [34] suffering from similar competitive adsorption mechanism followed by coke deposition, are reported. In addition to the temperature dependence, performing LA hydrogenation at higher H<sub>2</sub> pressure leads to quicker deactivation kinetics (see entries 1 and 8 in Table 2). It should be noted that the initial catalytic activity remains unchanged on increasing H<sub>2</sub> pressure while the stabilized activity increases with pressure. A few studies have highlighted the importance of different TiO<sub>2</sub> phases, i.e., anatase and rutile for LA hydrogenation [5,14]. Therefore, pure rutile phase of TiO<sub>2</sub> was used as a support (listed as entry 9 in Table 2) to investigate its catalytic activity. The initial activity observed with rutile phase was similar to the one observed with P25. In contrast, the deactivation was three-fold quicker and the stabilized activity was ~35% lower in case of rutile supported Ru catalyst as compared to P25. Our observations contradict the stability results for Ru/TiO<sub>2</sub> (rutile) for LA hydrogenation in presence of 1,4 dioxane as the solvent [14]. Hence, pure rutile support might be more susceptible to deactivation in presence of aqueous media and exhibits lower stabilized activity than the P25 support.

Fig. 6-D shows a linear relationship between the stabilized activity and LA feed concentration. For all the scenarios tested, the reactor was operated under integral conditions (i.e.,  $X_{LA} > 5\%$ ). The corresponding relationship between the stabilized catalytic activity and reaction order for LA concentration can be found in detail in Appendix D in SI. Based on this, a first-order LA dependence can be established. While it is difficult to determine the initial catalytic activity of the fresh catalyst (i.e.,  $a_0$ ) experimentally, this is determined by extrapolation of activity data to TOS = 0 h. As reported in Fig. 6-C, the initial catalytic activity is nearly independent of concentration, unlike the stabilized activity (shown in Fig. 6-D). Similar to our findings concerning initial LA hydrogenation activity, different studies have shown initial LA hydrogenation kinetics being independent of LA feed concentrations, even when they were performed at different ranges of temperatures and concentrations. One study was performed over a range of LA concentrations (0.15–0.45 M) at near ambient temperature (50 °C) using 5 wt% Ru/C [7], while the other at 50–130 °C using 0.5 wt% Ru/C [18]. Besides the initial catalytic activity, Piskun et al. [9] indicated the presence of internal diffusion limitations while using 5 wt% Ru/C at 130 °C. Therefore, additional experiments with differing catalyst particle sizes up to 200 µm were performed (see Figure S15). No significant differences were observed with catalytic performance during operation upon using particles in 32–53 and 53–80 µm range (for LA hydrogenation at 200 °C and 31 bar H<sub>2</sub> pressure exhibiting highest catalytic activity, a Weisz–Prater modulus of  $0.31 < 0.4$  is estimated in section F of SI), demonstrating that neither the catalyst deactivation nor LA hydrogenation kinetic were masked by internal diffusion limitations. Since the stabilized activity,  $a_{\infty}$ , follows a relationship with feed concentration, further inspection into reaction kinetics upon full deactivation or activity stabilization is done in Section 3.4.

### 3.3. Catalyst characterization

Different catalyst characterization techniques were used to establish the causes of deactivation during TOS for Ru/TiO<sub>2</sub>. Fig. 7 shows the results for XPS and TGA. Subplot C compares Ru particle size, obtained using TEM, of the fresh and spent 1 wt% Ru/TiO<sub>2</sub> from 100 mg catalyst loading experiments. The Ru particle size distribution shifts from a very narrow distribution with many sub-nm particles in the fresh catalyst to a much larger and broader distribution in the spent catalyst (i.e., from  $1.38 \pm 0.03$  nm to  $2.38 \pm 0.08$  nm mean particle sizes, respectively). Also, note the formation of a few larger agglomerates up to 10 nm (see Figure S2 in SI for TEM images). Unlike the results presented in this work, it was shown that Ru particle sintering does not occur while using 1,4-dioxane as a solvent [14]. Sintering generally occurs at high temperatures (>500 °C) but is known to occur at lower temperatures as well, especially in the presence of water [35]. While using 1 wt% Ru/TiO<sub>2</sub> at 200 °C, formation of larger aggregates of Ru after three days of operation results in approximately 60% decrease in the specific surface area of the exposed Ru particles (assuming ideal hemispherical shape). This is accompanied by 90% decrease in catalytic activity over the same period. Thus, this suggests that, while sintering occurs, it is likely not the only contributor to catalyst deactivation. Furthermore, deactivation experiments with 1 and 2 wt% Ru catalysts described in Fig. 5-A, show that deactivation does not significantly depend on Ru loading on the support in the present conditions (i.e., 200 °C used and aqueous phase).

Fig. 7-D shows the TGA results (performed under inert conditions, i.e., N<sub>2</sub>) of spent catalyst operated at 200 °C during different TOS (without washing). The mass loss experienced by all catalyst samples is within 2 to 3 wt%. The temperature regions where mass loss occurs correspond to the boiling points of GVL, levulinic and 4-hydroxy pentanoic acids, with the biggest contributor corresponding to GVL. This merely confirms the presence of these components on the surface of the spent unwashed catalyst (either as adsorbates, or deposited on the surface after drying of the liquid in the pores), and aligns with the high GVL selectivity obtained in these studies (i.e., ~95%). However, conclusions on strong adsorption by the organic acids and/or GVL on the catalyst surface cannot be easily drawn from these experiments. No major mass losses are observed at higher temperatures, suggesting absence coke on the catalyst surface. This is also in line with a full carbon balance during all experiments. Regardless of the species responsible for deactivation, coking or deposition on the catalyst can be ruled out as a pivotal deactivation mechanism in aqueous media. This can be explained by the indistinguishable mass loss during TG analysis of spent catalyst for different TOS, see Fig. 7-D. Additionally, carbon balance in all reported experiments remained  $100 \pm 2\%$ . Moreover, ICP relates no leaching of either Ru or Ti during operation. Similarly, no Ru leaching was reported in other works using TiO<sub>2</sub> as the support [8,10,14]. Besides the growth of Ru particle size, TEM images show a preservation of the



**Fig. 6.** Deactivation kinetics and catalytic activity for 1 wt% Ru/TiO<sub>2</sub>. Subplots (A) - Arrhenius relationship of deactivation kinetics and temperature using 2 wt% LA in water, (B) - Deactivation kinetics for different LA concentration, (C) - Initial catalytic activity (obtained via fitting) and (D) - Stabilized catalytic activity for different LA concentrations. Kinetic values shown in subplots (B), (C) and (D) are obtained at 200 °C.

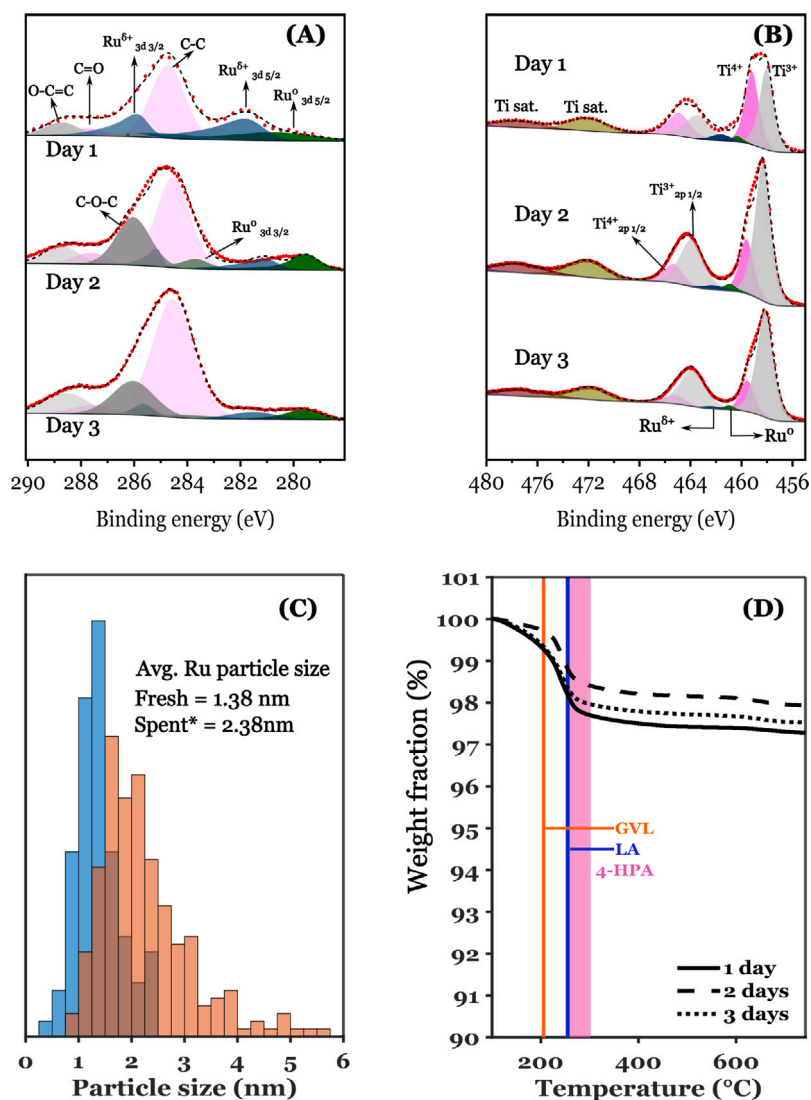


**Fig. 7.** Spent catalyst characterization of 1 wt% Ru/TiO<sub>2</sub>. Subplots (A) and (B) - XPS spectra for different time-on-stream for Ru3d and Ti2p, respectively. (C) - Particle size distribution for fresh and spent (\* - three days of operation) catalysts represented by blue and orange bars, respectively. (D) - TGA curve for different time-on-stream. Purple line represents boiling point of GVL while the beginning of the green bar and its width represent boiling point of LA and uncertainty related to boiling point of 4-HPA.

crystalline structure of TiO<sub>2</sub> support. This is also confirmed by XRD patterns showing similar peaks for fresh and spent samples (see Figure

S4 in SI). Therefore, TiO<sub>2</sub> presents a favorable alternative in terms of conserving its crystalline structure as a support.



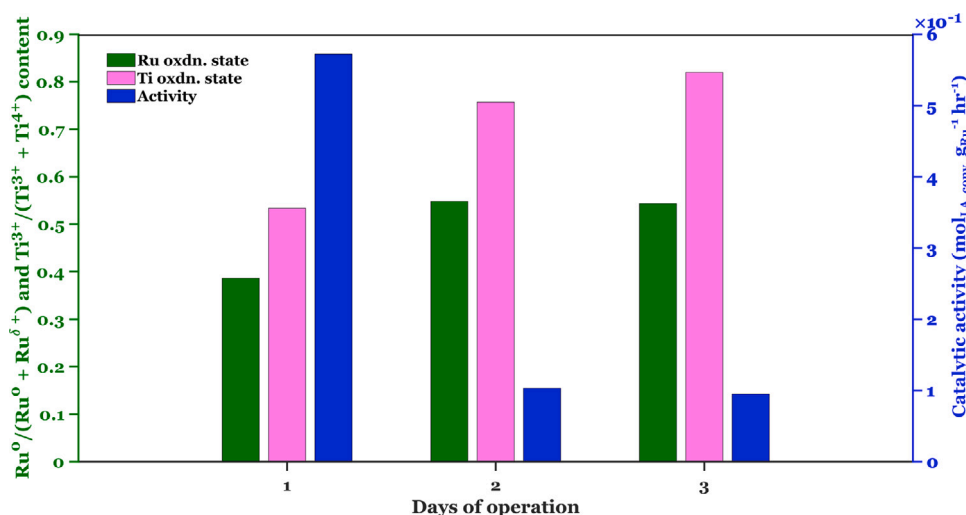


Fig. 8. Proportion of Ru<sup>0</sup> and Ti<sup>4+</sup> on the catalyst surface, and average catalytic activity with different days of operation. Reaction conditions:  $T = 200\text{ }^{\circ}\text{C}$ ;  $P_{\text{H}_2} = 31\text{ bar}$ ;  $W_{\text{cat}} = 0.1\text{ g}$ ;  $W_{\text{SiC}} = 3.9\text{ g}$ ;  $Q_{\text{feed}} = 1\text{ mL min}^{-1}$ ;  $Q_{\text{H}_2} = 40\text{ N m L min}^{-1}$ ;  $\text{WHSV} = 600\text{ g}_{\text{feed}}\text{ g}_{\text{cat}}^{-1}\text{ h}^{-1}$ .

XPS measurements were conducted to gain additional insights into the change in catalyst structure on the fresh and spent catalysts with different TOS. The fresh catalyst exhibits a distinct shoulder in the region between 280–282 eV (Figure S7 in SI), indicative of unreduced Ru in its oxide or hydroxide form (i.e., RuO<sub>2</sub> or Ru(OH)<sub>3</sub>) for Ru 3d core level. This is assigned to the oxidation of metallic Ru upon exposure to ambient [36]. The resolution of the Ti 2p core level is more complex due to the overlap with Ru 3p spectra. Therefore, commercially available TiO<sub>2</sub> powder, i.e., P-25, was used to obtain fitting constraints for Ti<sup>4+</sup> peak model (more details can be found in subsection B.3.1 of SI). The surface Ti species of the fresh catalyst undergo reduction from Ti<sup>4+</sup> to Ti<sup>3+</sup>, the latter 2p<sub>3/2</sub> component was detected at  $457.9 \pm 0.3\text{ eV}$ . The content of Ru<sup>0</sup> and Ti<sup>3+</sup> relative to that of their respective higher oxidation states increase with time of operation, as shown in Fig. 7-A and B, respectively. In the case of Ti, the FWHM for spent catalysts falls under the range of 1.45 to 1.7 eV (peak broadening from 1.1 eV observed with fresh TiO<sub>2</sub>), demonstrating the presence of an additional oxidation state of Ti other than 4+.

The day-averaged LA hydrogenation activity is plotted against Ru<sup>0</sup>/(Ru<sup>0</sup> + Ru<sup>δ+</sup>) and Ti<sup>3+</sup>/(Ti<sup>4+</sup> + Ti<sup>3+</sup>), shown in Fig. 8. Due to a quick deactivation within the first day of operation (approximately 0.25 h<sup>-1</sup> resulting in loss of 90% catalytic activity at 200 °C), the LA hydrogenation activity remains relatively unchanged for days 2 and 3. Similarly, the values of Ru<sup>0</sup>/(Ru<sup>0</sup> + Ru<sup>δ+</sup>) and Ti<sup>3+</sup>/(Ti<sup>4+</sup> + Ti<sup>3+</sup>) remain stable over this period, indicating that the reduction of Ru<sup>δ+</sup> surface species to Ru<sup>0</sup>, and Ti<sup>4+</sup> to Ti<sup>3+</sup> does not proceed to completion. LA hydrogenation activity and the change in Ru and Ti oxidation states are very much alike, reaching stable values after the initial deactivation. These observations are corroborated by XPS analysis for the spent catalyst, which reveal the existence of both Ru<sup>δ+</sup> and Ru<sup>0</sup> oxidation states after continuous operation of >100 h. We hypothesize an equilibrium between these Ru species, as their relative content remains relatively unchanged when comparing catalytic beds tested for 2, 3 and 20 days of operation. The relative content of Ru<sup>δ+</sup> with respect to total Ru remains within 48 to 60%, when increasing Ru loadings from 1 to 2 wt% Ru, respectively. The discrepancy can be attributed to the assignment of different Ru oxidation states (ranging from 1+ to 4+) cumulatively to a single Ru<sup>δ+</sup> species. Although the chemical environment on the catalyst surface undergoes extensive reduction, the crystalline structure (determined by XRD, see Figure S3) remains essentially unchanged, suggesting preservation of Ti<sup>4+</sup> in the bulk of the catalyst.

Several studies using supported RuO<sub>2</sub> catalyst have investigated the activity of various Ru oxidation states during LA hydrogenation. Kasar

Table 3

Ru dispersion and TOF at the beginning of time-on-stream and after activity stabilization for LA hydrogenation performed at 200 °C and 31 bar H<sub>2</sub>.

Catalyst	Ru dispersion %	Ru surface area m <sup>2</sup> g <sub>cat</sub> <sup>-1</sup>	X <sub>LA</sub> %	TOF <sup>a</sup> h <sup>-1</sup>
1 wt% Ru/TiO <sub>2</sub> (fresh)	11.25	0.41	90	8582
1 wt% Ru/TiO <sub>2</sub> (spent)	1.14	0.04	9.5	8415
2 wt% Ru/TiO <sub>2</sub> (fresh)	4.17	0.30	95	11,575
2 wt% Ru/TiO <sub>2</sub> (spent)	1.06	0.08	43	21,788

<sup>a</sup> TOF calculated based on dispersion of Ru obtained via CO pulse chemisorption.

et al. [2] show an increase in Ru<sup>0</sup> content in the spent catalyst compared to the fresh catalysts using Ru and Ni in conjunction. Recently, Abusuek et al. [37] and Gundekari et al. [15] have demonstrated the ability of Ru oxides to catalyze LA hydrogenation. Furthermore, the latter study revealed the necessity of adsorbed water molecules to enable in-situ Ru reduction for catalyzing LA hydrogenation. In light of such reports, unreduced Ru/TiO<sub>2</sub> was used for LA hydrogenation at 200 °C and 31 bar H<sub>2</sub> pressure. Our results showed negligible hydrogenation activity (see Figure S16 in SI), with a meager 4% LA conversion followed by 2% on the next day. Hence, Ru<sup>4+</sup> or Ru<sup>δ+</sup> cannot be the sole active species for LA hydrogenation. Although the reduction protocol for the catalyst involved H<sub>2</sub> treatment at 450 °C (i.e., higher than the reaction conditions), subsequent exposure to ambient air during transfer to the reactor, results in the oxidation of Ru<sup>0</sup> to Ru<sup>4+</sup>. Regardless, the catalytic run with unreduced Ru and ex-situ XPS analysis of Ru/TiO<sub>2</sub> with different TOS suggests that a combination of both Ru<sup>0</sup> and Ru<sup>δ+</sup> states is necessary for LA hydrogenation while using TiO<sub>2</sub> as the support.

Table 3 depicts Ru dispersion before and after catalytic runs for the different Ru loadings. The reduction in Ru dispersion with higher mass loading indicates that the Ru nanoparticles are mobile and agglomerate to form larger clusters at higher Ru loadings. In case of 1 wt% Ru loadings, the inherent catalytic activity, expressed as turnover frequency (TOF) in h<sup>-1</sup>, remains similar. This signifies that the inherent catalytic activity is retained and is very well defined by the amount of Ru being exposed. Since the deactivation of the catalyst occurs extensively due to sintering of Ru nanoparticles assisted by the presence of LA in the feed, the exposed metallic surface area gets reduced, thereby reducing the catalytic activity per gram of catalyst. In case of higher Ru loadings, i.e., 2 wt% Ru/TiO<sub>2</sub>, the initial inherent activity of the catalyst is difficult to estimate as almost complete LA conversion can be obtained by 1 wt% Ru loading (see first entry of Table 3). Regardless, the TOF

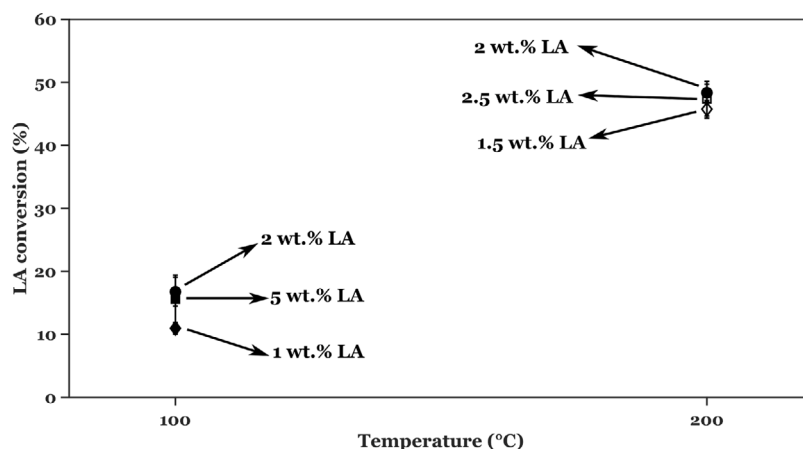


Fig. 9. LA conversion with different concentration upon activity stabilization. Reaction conditions:  $P_{H_2} = 31$  bar;  $W_{cat} = 0.2$  g;  $W_{SiC} = 3.8$  g;  $Q_{feed} = 1$  mL min<sup>-1</sup>;  $Q_{H_2} = 40$  N m L min<sup>-1</sup>; WHSV = 300 g<sub>feed</sub> g<sub>cat</sub><sup>-1</sup> h<sup>-1</sup>.

in case of fresh 2 wt% Ru is higher than 25% of its lower Ru loading counterpart. After reaching stabilized activity, the TOF for higher Ru loading is approximately three-fold of 1 wt% Ru (spent). While the exposed Ru surface area per  $g_{Ru}$  for both the spent catalysts remains the same,  $X_{LA}$  obtained with higher Ru loading is at least four times greater than 1 wt% Ru (spent).

### 3.4. Kinetics of LA hydrogenation on deactivated catalyst

Several studies on LA hydrogenation with Ru/C [7,9] catalysts report a zero-order kinetics with respect to LA concentration. Furthermore, few other studies using MnO<sub>6</sub> [19] and montmorillonite (MMT) clay [2] as supports in batch reactors report a fractional order dependence of LA. This behavior is observed with fresh catalysts at the start of time-on-stream operations. Nonetheless, there are no studies on LA hydrogenation kinetics after activity stabilization is achieved. Hence, in our work, the catalytic bed of 200 mg 1 wt% Ru/TiO<sub>2</sub> was operated continuously for 120 h to achieve stable activity (Fig. 5-B). Following deactivation, kinetic investigation was performed for order dependence within the stable activity region for different feed LA concentrations, as shown in Fig. 9. Similar LA conversion was observed for different feed concentrations at 100 °C, which is an expected trend for first-order kinetics (see Appendix D in SI). Supporting experiments at 200 °C led to equal LA conversion with feed concentration ranging from 1.5 to 2.5 wt%, thereby confirming first-order dependence. The activity resulting from 2 wt% LA in feed was comparable to that observed at 120 h of TOS at similar conditions, corroborating catalytic stability. Follow-up experiments with different WHSV (i.e., this time, varying flow rates) lead to the predicted performance based on first-order kinetics (see Appendix D in SI). The revelation of first-order reactant dependence unveils opportunities to enhance productivity, unlike zero-order kinetics. This can boost productivity to 13.7 g<sub>GVL</sub> g<sub>cat</sub><sup>-1</sup> h<sup>-1</sup> with 10 wt% LA over 100 mg 2 wt% Ru/TiO<sub>2</sub>. However, higher LA concentrations present a risk of Ru leaching due to high pK<sub>a</sub>, similar to acetic acid.

In addition to the dependence of LA concentration on reaction kinetics, different works report fractional order dependence of hydrogen pressures, ranging from 0.4 to 1 [7,9,18,19,38]. To investigate this, we used 21 and 31 bar of H<sub>2</sub> pressures with different LA concentrations (i.e., 1 and 2 wt%) at 100 °C. Our results indicate a reaction order of  $0.53 \pm 0.10$  with respect to hydrogen after the activity stabilization. Therefore, the reaction kinetics can be expressed as  $k c_{LA} c_{H_2}^{0.5}$ .

On the basis of the first-order dependence of LA hydrogenation kinetics, the activation energy for the first step in the reaction network of LA to GVL can be approximated. A detailed explanation of this can be found in Appendix E of SI. The activation energy for LA hydrogenation

Table 4

Activation energy values reported in various works for Ru catalyzed LA hydrogenation.

Catalyst	Activation energy $E_a$ kJ mol <sup>-1</sup>	Reference
5 wt% Ru/C	48 ± 5	[7]
0.5–5 wt% Ru-Ni/MMT	44.1	[2]
3 wt% Ru/C	54.9 ± 2.7	[9]
5 wt% Ru/C	68.1	[38]
1 wt% Ru/OMS	49.2	[19]
1 wt% Ru/TiO <sub>2</sub>	54.7	[39]
0.2–1 wt% Pd-Ru/TiO <sub>2</sub>	37.3	[39]
0.83 wt% Ru/TiO <sub>2</sub>	43.4	[40]
1 wt% Ru/TiO <sub>2</sub>	23	This work

to 4-HPA is about 23 kJ mol<sup>-1</sup>, derived from kinetic data at 100 and 200 °C. Reported values range from 43 to 68 kJ mol<sup>-1</sup> (data based on fresh catalysts), with this work reporting one of the lowest Table 4. The activation energy in this study is roughly half the lowest reported, raising concerns about internal diffusion limitations. The Weisz–Prater modulus was evaluated and confirmed that kinetic data were free of such limitations. External mass transfer limitations were evaluated using Mears criterion, as shown in section F of SI. A Mears number of  $0.07 < 0.15$  for LA hydrogenation at 200 °C and 31 bar H<sub>2</sub> pressure at the beginning of time-on-stream, exhibiting highest catalytic activity, confirms the absence of external mass transfer limitations in this work. Furthermore, as the volumetric flow rates were reduced, leading to increased contact times, an increase in LA conversion was observed (see Figure S18), confirming kinetic limitations at 200 °C when performing kinetic studies on the stabilized catalyst.

## 4. Discussion

The results presented in this work have shown that Ru/TiO<sub>2</sub> is an effective catalyst for LA hydrogenation in aqueous media. Higher reaction temperatures lead to greater GVL selectivity via an auto-catalytic (partly) homogeneously catalyzed ring-closure of the intermediate, 4-HPA. Regardless of the reaction conditions, Ru/TiO<sub>2</sub> undergoes deactivation. However, after a certain period of around 5–15 h depending on conditions, the catalyst achieves stable activity. Deactivation kinetics are highly dependent on process conditions (i.e., temperature, feed LA concentration and catalyst loadings), pointing at competitive adsorption of carboxylic acids on the hydrogenation sites as plausible cause of activity drop. TGA results show the absence of coke deposits on the catalyst surface.

TEM, CO chemisorption and XPS analysis show Ru particle sintering and a change in oxidation state of Ru and Ti species. These changes

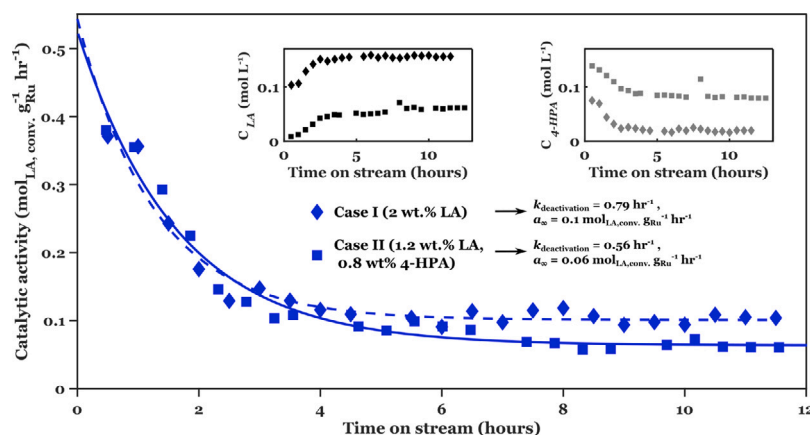


Fig. 10. Catalyst activity profiles vs. time using 1 wt% Ru/TiO<sub>2</sub> using differing carboxylic acid content in the feed. Reaction conditions:  $T = 100\text{ }^{\circ}\text{C}$ ;  $P_{\text{H}_2} = 45\text{ bar}$ ;  $W_{\text{cat}} = 0.1\text{ g}$ ;  $W_{\text{SiC}} = 3.8\text{ g}$ ;  $Q_{\text{feed}} = 1\text{ mL min}^{-1}$ ;  $Q_{\text{H}_2} = 40\text{ N m L min}^{-1}$ ;  $\text{WHSV} = 600\text{ g}_{\text{feed}}\text{ g}_{\text{cat}}^{-1}\text{ h}^{-1}$ . Case I: 2 wt% LA; Case II: 1.2 wt% LA and 0.8 wt% 4-HPA.

take place in the initial hours of TOS, in parallel to the evident decrease in catalytic activity. Additional Ru dispersion measurements with RuO<sub>2</sub>/TiO<sub>2</sub> in presence of LA reveals minimal change in Ru dispersion, demonstrating that Ru<sup>δ+</sup> do not form clusters. Kinetic analysis and relatively higher Ru dispersion (4.5%–5%) observed in absence of LA in the aqueous feed than in presence of LA (1.2%) indicates that carboxylic acids may initiate deactivation by competing for catalytic sites or promoting the mobilization of Ru<sup>0</sup> species (as shown for liquid phase reaction with Pt and Pd [41]) and thus sintering. Hence, at the beginning of the time-on-stream operation, the kinetics for sintering are quicker and the Ru particles may reach a ‘critical radius’ as shown by Houk et al. [42] and Finney et al. [28], thereby slowing down the deactivation rate near the stabilized activity region. With evidences of Ru particle size growth, our analysis show that sintering cannot be the sole cause of deactivation. Our results reported in Fig. 5 showing slower deactivation with higher Ru loadings support the idea of competitive adsorption. Liu et al. [14] demonstrated that Ru overcoating from adsorbate induced surface reduction of TiO<sub>2</sub>, confirmed by XPS data in our work, creates strong metal-support interactions that reduce catalyst activity.

To further resolve the identity of the carboxylic acid causing deactivation, two control experiments with same carboxylic acid content in the feed were performed. Fig. 10 shows the catalytic activity profile of two different 1 wt% Ru/TiO<sub>2</sub> catalytic beds with TOS at 100 °C (Case I: Model feed 2 wt% LA and Case II: Mixed feed consisting of 1.2 and 0.8 wt% LA and 4-HPA, respectively). The catalyst deactivation rate is higher for case I than II, i.e.,  $0.79 \pm 0.1$  vs.  $0.56 \pm 0.1\text{ h}^{-1}$ , respectively. Similar concentration of carboxylic acid was detected at the reactor outlet for both cases (0.15–0.17 mol L<sup>-1</sup>). In particular, the concentration of 4-HPA is approximately 6–7 times higher in case II than case I. Therefore, an overall higher 4-HPA concentration is experienced by the catalytic bed with the mixed feed, resulting in slower loss of catalytic activity. The observation of quicker deactivation with the model LA (i.e., higher LA concentration) feed is also in line with a linear relationship between LA and deactivation kinetics observed at 200 °C.

It is trivial that higher temperature enhances the inherent catalytic activity due to Arrhenius dependence, resulting in greater LA conversion and an overall lower carboxylic acid (specifically, LA) content experienced by the catalytic bed. These findings with a mixed feed (LA and 4-HPA) agree well with the observation of decrease in deactivation rate with increase in reaction temperature. Additionally, in accordance with observations made in Section 2.5, the initial catalytic activity is similar for case I and II while the stabilized activity scales with LA concentration and representative of first-order dependence on concentration of LA.

In order to elucidate the nature of the active sites, XPS data reveal a change in the oxidation state of Ru from  $\delta+$  to metallic state with increasing TOS, parallel to the drop in catalytic activity exhibited by the same catalyst. When an unreduced form of the same catalyst was used, insignificant LA conversion was observed for the entire TOS. Therefore, the existence of both Ru<sup>δ+</sup> and Ru<sup>0</sup> seems to be necessary for LA hydrogenation. Interestingly, the use of stronger organic acids, i.e., formic and lactic acid ( $\text{pK}_a \sim 3.7$ ), leads to decrease in LA hydrogenation activity. In the former case, no LA conversion was observed while in case of lactic acid, lower LA hydrogenation activity (see Figure S19 in SI) is observed as compared to the feed comprising of LA and 4-HPA. These observations are in line with other works demonstrating sudden loss of catalytic activity while switching to feed containing formic acid as an impurity during LA hydrogenation [43]. Several works involving Ru catalyzed formic acid dehydrogenation show the presence of Ru<sup>+</sup> or Ru<sup>2+</sup> being beneficial, albeit under homogeneous conditions [44,45]. Recently, Xue et al. [46] have shown that formic acid dehydrogenation proceeds via formate pathway. The competitive adsorption of carboxylate species R–COO\* on either Ru<sup>0</sup> or Ru<sup>δ+</sup> sites can lead to reduced LA hydrogenation activity. Insights from similar in-situ and operando techniques may further support this work [47]. However, the application of operando techniques for gas–liquid–solid catalytic reaction remains limited due to the solvent signal [48].

In addition, the study investigates the kinetics of deactivation as well as the kinetics of LA after stabilized activity. This study revealed that higher Ru loadings in the reactor can mask deactivation in a flow-through reactor during the initial TOS (<3 h in Figure S12). In addition, performing kinetic analysis in the initial lifespan of the catalyst may also lead to a falsified relationship of reaction order with respect to LA. Numerous works on LA hydrogenation to GVL reveal zero-order LA dependence [7,9,18], while this work shows that this is only valid for the beginning of TOS. Besides, this work investigated LA hydrogenation kinetics after achieving catalyst stabilization. While most of the reported works performed kinetic studies with fresh catalyst (TOS < 3 h), we illustrate that reaction kinetics transition from a zero-order to first-order dependence on LA. Half-order dependency was found for H<sub>2</sub>. Other studies have shown that using higher Ru loading (i.e., 3 wt% Ru/C) leads to internal diffusion limitations at 70–130 °C [9]. Operating within such regime leads to misrepresentation of kinetics, halving of the true activation energy and changing of reaction order from  $n$  to  $(n+1)/2$ . In our work, both experimental and numerical validation for absence of internal diffusion limitations were performed (see Figure S15 and Appendix F in SI). However, particle sizes above 100 μm and Ru loadings greater than 2 wt% may be conducive to internal diffusion limitation.

## 5. Conclusion

This study examines LA hydrogenation to GVL in a flow reactor with TiO<sub>2</sub>-supported Ru catalysts, emphasizing the significance of deactivation in the process. A notable decline in catalytic activity is observed within the initial hours of operation. Despite this deactivation, the catalyst consistently attains a stabilized region of activity. Neither coking nor metal leaching was found to play a significant role in this process. Conversely, the occurrence of mild sintering of Ru particles and reduction of surface Ru and Ti species have been identified using TEM and XPS, respectively. Analysis of the deactivation kinetics reveals that increasing feed concentration accelerates activity loss, while operating at higher reaction temperature decelerates deactivation. Furthermore, the deactivation rate is unaffected by Ru loading (per gram catalyst). This is in contrast to the expected behavior for sintering, which usually increases at higher temperatures and greater Ru loadings. Thus, the surface reduction process and the presence of carboxylic acids appear to be relevant to the deactivation process. Reaction conditions, i.e., high partial pressure of water and hydrogen are favorable reduction of Ru<sup>δ+</sup> to Ru<sup>0</sup>. Still, the existence of both Ru<sup>δ+</sup> and Ru<sup>0</sup> seems necessary for LA hydrogenation. Remarkably, doubling the catalyst mass in the reactor during high temperature operation (200 °C), not only masks early deactivation by operating under full conversion, but also reduces deactivation kinetics, resulting in greater stabilized activity. This observation can be attributed to the reduced concentration of carboxylic acids, which has been demonstrated to play a role in the deactivation mechanism. Control experiments with differing distribution of LA and 4-HPA and keeping the overall carboxylic acid content constant in the liquid feed conclusively show that LA is predominantly responsible for catalyst deactivation. Finally, a kinetic study for LA hydrogenation in the region of stabilized activity reveals first-order kinetic dependence on LA. The sensitivity of catalyst with temperature in the stable region is rather low as compared to that observed in other reported works. Our study on LA hydrogenation underscores the importance of understanding reaction kinetics during deactivation and activity stabilization. Delving into kinetic analysis with a catalyst in its stable state is crucial for informed reactor design and equipment selection in the chemical industry.

## CRediT authorship contribution statement

**Adarsh Patil:** Writing – original draft, Formal analysis, Data curation, Conceptualization. **Amin Delparish:** Writing – review & editing, Formal analysis. **Remy Creemers:** Formal analysis, Data curation. **John van der Schaaf:** Writing – review & editing, Supervision. **Fernanda Neira D'Angelo:** Writing – review & editing, Writing – original draft, Supervision, Funding acquisition, Formal analysis.

## Declaration of competing interest

The authors declare that they have no known competing financial interests or personal relationships that could have appeared to influence the work reported in this paper.

## Acknowledgment

This project has received funding from the European Union's Horizon 2020 research and innovation programme under grant agreement No. 101006618.

## Appendix A. Supplementary data

Supplementary material related to this article can be found online at <https://doi.org/10.1016/j.cej.2025.165037>.

## Data availability

Data will be made available on request.

## References

- [1] M. Mani, M. Mariyaselvakumar, A. Samikannu, A.B. Panda, L.J. Konwar, J.-P. Mikkola, Continuous hydrocyclization of aqueous levulinic acid to  $\gamma$ -valerolactone over bi-functional ru/nbopo4/sba-15 catalyst under mild conditions, *Appl. Catal. A: Gen.* 643 (2022) 118744.
- [2] G.B. Kasar, R.S. Medhekar, P.N. Bhosale, C.V. Rode, Kinetics of hydrogenation of aqueous levulinic acid over bimetallic ru-ni/mmt catalyst, *Ind. Eng. Chem. Res.* 58 (2019) 19803–19817.
- [3] K. Hengst, M. Schubert, H.W. Carvalho, C. Lu, W. Kleist, J.-D. Grunwaldt, Synthesis of  $\gamma$ -valerolactone by hydrogenation of levulinic acid over supported nickel catalysts, *Appl. Catal. A: Gen.* 502 (2015) 18–26.
- [4] L.F. Sosa, V.T. da Silva, P.M. de Souza, Hydrogenation of levulinic acid to  $\gamma$ -valerolactone using carbon nanotubes supported nickel catalysts, *Catal. Today* 381 (2021) 86–95.
- [5] A.M. Ruppert, J. Grams, M. Jędrzejczyk, J. Matras-Michalska, N. Keller, K. Ostojka, P. Sautet, Titania-supported catalysts for levulinic acid hydrogenation: Influence of support and its impact on  $\gamma$ -valerolactone yield, *ChemSusChem* 8 (2015) 1497–1497.
- [6] M. Al-Naji, M. Popova, Z. Chen, N. Wilde, R. Gläser, Aqueous-phase hydrogenation of levulinic acid using formic acid as a sustainable reducing agent over pt catalysts supported on mesoporous zirconia, *ACS Sustain. Chem. Eng.* 8 (2019) 393–402.
- [7] O. Abdelrahman, A. Heyden, J. Bond, Analysis of kinetics and reaction pathways in the aqueous-phase hydrogenation of levulinic acid to form  $\gamma$ -valerolactone over ru/c, *ACS Catal.* 4 (2014) 1171–1181.
- [8] O. Abdelrahman, H.Y. Luo, A. Heyden, Y. Román-Leshkov, J.Q. Bond, Toward rational design of stable, supported metal catalysts for aqueous-phase processing: Insights from the hydrogenation of levulinic acid, *J. Catalysis* 329 (2015) 10–21.
- [9] A. Piskun, H. van de Bovenkamp, C. Rasrendra, J. Winkelman, H. Heeres, Kinetic modeling of levulinic acid hydrogenation to  $\gamma$ -valerolactone in water using a carbon supported ru catalyst, *Appl. Catal. A: Gen.* 525 (2016) 158–167.
- [10] A.S. Piskun, J.E. de Haan, E. Wilbers, H.H. van de Bovenkamp, Z. Tang, H.J. Heeres, Hydrogenation of levulinic acid to  $\gamma$ -valerolactone in water using millimeter sized supported ru catalysts in a packed bed reactor, *ACS Sustain. Chem. Eng.* 4 (2016) 2939–2950.
- [11] A.S. Piskun, Catalytic Conversion of Levulinic Acid to  $\gamma$ -Valerolactone using Supported Ru Catalysts: from Molecular to Reactor Level (Ph.D. thesis), University of Groningen, 2016.
- [12] M. Varkolu, V. Velpula, D.R. Burri, S.R.R. Kamaraju, Gas phase hydrogenation of levulinic acid to  $\gamma$ -valerolactone over supported ni catalysts with formic acid as hydrogen source, *New J. Chem.* 40 (2016) 3261–3267.
- [13] J. Ftouni, A. Muñoz-Murillo, A. Goryachev, J.P. Hofmann, E.J.M. Hensen, L. Lu, C.J. Kiely, P.C.A. Bruijninx, B.M. Weckhuysen, ZrO<sub>2</sub> is preferred over TiO<sub>2</sub> as support for the ru-catalyzed hydrogenation of levulinic acid to  $\gamma$ -valerolactone, *ACS Catal.* 6 (2016) 5462–5472.
- [14] F. Liu, J. Ftouni, P.C.A. Bruijninx, B.M. Weckhuysen, Phase-dependent stability and substrate-induced deactivation by strong metal-support interaction of ru/TiO<sub>2</sub> catalysts for the hydrogenation of levulinic acid, *ChemCatChem* 11 (2019) 2079–2088.
- [15] S. Gundekari, K. Srinivasan, Hydrous ruthenium oxide: A new generation remarkable catalyst precursor for energy efficient and sustainable production of  $\gamma$ -valerolactone from levulinic acid in aqueous medium, *Appl. Catal. A: Gen.* 569 (2019) 117–125.
- [16] M.B. Shemfe, B. Fidalgo, S. Gu, Heat integration for bio-oil hydroprocessing coupled with aqueous phase steam reforming, *Chem. Eng. Res. Des.* 107 (2016) 73–80.
- [17] R. Junsittiwate, T.R. Srinophakun, S. Sukpancharoen, Techno-economic, environmental, and heat integration of palm empty fruit bunch upgrading for power generation, *Energy Sustain. Dev.* 66 (2022) 140–150.
- [18] A. Hommes, A.J. ter Horst, M. Koeslag, H.J. Heeres, J. Yue, Experimental and modeling studies on the ru/c catalyzed levulinic acid hydrogenation to  $\gamma$ -valerolactone in packed bed microreactors, *Chem. Eng. J.* 399 (2020) 125750.
- [19] J. Molleti, M.S. Tiwari, G.D. Yadav, Novel synthesis of ru/oms catalyst by solvent-free method: Selective hydrogenation of levulinic acid to valerolactone in aqueous medium and kinetic modelling, *Chem. Eng. J.* 334 (2018) 2488–2499.
- [20] J. Lange, Renewable feedstocks: The problem of catalyst deactivation and its mitigation, *Angew. Chem. Int. Ed.* 54 (2015) 13186–13197.
- [21] S. Bagheri, N.M. Julkapli, S.B.A. Hamid, Titanium dioxide as a catalyst support in heterogeneous catalysis, *Sci. World J.* 2014 (2014) 1–21.
- [22] Z.M. Shakor, E.N. Al-Shafei, The mathematical catalyst deactivation models: a mini review, *RSC Adv.* 13 (2023) 22579–22592.
- [23] J. Lange, R. Price, P.M. Ayoub, J. Louis, L. Petrus, L. Clarke, H. Gosselink, Valeric biofuels: A platform of cellulosic transportation fuels, *Angew. Chem. Int. Ed.* 49 (2010) 4479–4483.



- [24] M. Al-Naji, J.V. Aelst, Y. Liao, M. d'Hullian, Z. Tian, C. Wang, R. Gläser, B.F. Sels, Pentanoic acid from  $\gamma$ -valerolactone and formic acid using bifunctional catalysis, *Green Chem.* 22 (2020) 1171–1181.
- [25] S.G. Wettstein, J.Q. Bond, D.M. Alonso, H.N. Pham, A.K. Datye, J.A. Dumesic, Rusn bimetallic catalysts for selective hydrogenation of levulinic acid to  $\gamma$ -valerolactone, *Appl. Catal. B: Environ.* 117–118 (2012) 321–329.
- [26] M.G. Al-Shaal, M. Calin, I. Delidovich, R. Palkovits, Microwave-assisted reduction of levulinic acid with alcohols producing  $\gamma$ -valerolactone in the presence of a ru/c catalyst, *Catal. Commun.* 75 (2016) 65–68.
- [27] A.M.R. Galletti, C. Antonetti, V.D. Luise, M. Martinelli, A sustainable process for the production of  $\gamma$ -valerolactone by hydrogenation of biomass-derived levulinic acid, *Green Chem.* 14 (2012) 688.
- [28] E.E. Finney, R.G. Finke, Catalyst sintering kinetics data: Is there a minimal chemical mechanism underlying kinetics previously fit by empirical power-law expressions—and if so, what are its implications? *Ind. Eng. Chem. Res.* 56 (2017) 10271–10286.
- [29] D. Thakur, R. Tiggelaar, Y. Weber, J. Gardeniers, L. Lefferts, K. Seshan, Ruthenium catalyst on carbon nanofiber support layers for use in silicon-based structured microreactors. part ii: Catalytic reduction of bromate contaminants in aqueous phase, *Appl. Catal. B: Environ.* 102 (2011) 243–250.
- [30] P. Yin, S. Hu, K. Qian, Z. Wei, L.-L. Zhang, Y. Lin, W. Huang, H. Xiong, W.-X. Li, H.-W. Liang, Quantification of critical particle distance for mitigating catalyst sintering, *Nat. Commun.* 12 (2021) Not available.
- [31] N. Baylan, Removal of levulinic acid from aqueous solutions by clay nano-adsorbents: Equilibrium, kinetic, and thermodynamic data, *Biomass Convers. Biorefinery* 10 (2020) 1291–1300.
- [32] Y.Y. Baojian Liu, Q. Ren, Parallel pore and surface diffusion of levulinic acid in basic polymeric adsorbents, *J. Chromatogr. A* 1132 (2006) 190–200.
- [33] A.G. Sani, H.A. Ebrahim, M. Azarhoosh, 8-lump kinetic model for fluid catalytic cracking with olefin detailed distribution study, *Fuel* 225 (2018) 322–335.
- [34] R.B. Demuner, J.G.S.S. Maia, A.R. Secchi, P.A. Melo, R.W. do Carmo, G.S. Gusmão, Modeling of catalyst deactivation in bioethanol dehydration reactor, *Ind. Eng. Chem. Res.* 58 (2019) 2717–2726.
- [35] C. Bartholomew, Mechanisms of catalyst deactivation, *Appl. Catal. A: Gen.* 212 (2001) 17–60.
- [36] P.G.J. Koopman, Ruthenium Hydrogenation Catalysts: Activation Characterization Application (Ph.D. thesis), TU Delft, 1980.
- [37] D.A. Abusuek, O.P. Tkachenko, A.V. Bykov, A.I. Sidorov, V.G. Matveeva, M.G. Sulman, L.Z. Nikoshvili, Zsm-5 as a support for ru-containing catalysts of levulinic acid hydrogenation: Influence of the reaction conditions and the zeolite acidity, *Catal. Today* 423 (2023) 113885.
- [38] A.B. Jain, P.D. Vaidya, Kinetics of the ruthenium-catalyzed hydrogenation of levulinic acid to  $\gamma$ -valerolactone in aqueous solutions, *Can. J. Chem. Eng.* 94 (2016) 2364–2372.
- [39] G. Xu, C. Li, T. Deng, C. Wang, Y. Zhang, Y. Fu, Kinetic studies on the impact of pd addition to ru/tio<sub>2</sub> catalyst: Levulinic acid to  $\gamma$ -valerolactone under ambient hydrogen pressure, *Ind. Eng. Chem. Res.* 59 (2020) 17279–17286.
- [40] X. Gao, S. Zhu, M. Dong, J. Wang, W. Fan, Ru nanoparticles deposited on ultrathin tio<sub>2</sub> nanosheets as highly active catalyst for levulinic acid hydrogenation to  $\gamma$ -valerolactone, *Appl. Catal. B: Environ.* 259 (2019) 118076.
- [41] J.A. Lopez-Ruiz, Decarbonylation of Carboxylic Acids over Supported Metal Catalysts (Ph.D. thesis), University of Virginia, 2014.
- [42] L.R. Houk, S.R. Challa, B. Grayson, P. Fanson, A.K. Datye, The definition of critical radius for a collection of nanoparticles undergoing ostwald ripening, *Langmuir* 25 (2009) 11225–11227.
- [43] H.C. Genuino, H.H. van de Bovenkamp, E. Wilbers, J.G.M. Winkelman, A. Goryachev, J.P. Hofmann, E.J.M. Hensen, B.M. Weckhuysen, P.C.A. Bruijninx, H.J. Heeres, Catalytic hydrogenation of renewable levulinic acid to  $\gamma$ -valerolactone: Insights into the influence of feed impurities on catalyst performance in batch and flow reactors, *ACS Sustain. Chem. Eng.* 8 (2020) 5903–5919.
- [44] C. Guan, D.-D. Zhang, Y. Pan, M. Iguchi, M.J. Ajitha, J. Hu, H. Li, C. Yao, M.-H. Huang, S. Min, J. Zheng, Y. Himeda, H. Kawanami, K.-W. Huang, Dehydrogenation of formic acid catalyzed by a ruthenium complex with an n, n'-diimine ligand, *Inorg. Chem.* 56 (2017) 438–445, PMID: 27983821.
- [45] J.M. Edor, M.C. Joseph, J.H. Jordaan, H.C.M. Vosloo, A.J. Swarts, Formic acid dehydrogenation catalysis using novel pyridyl-formamidine half-sandwich ruthenium(ii) complexes, *Appl. Organomet. Chem.* 39 (2025).
- [46] G. Xue, Y. Jiao, X. Li, T. Lin, C. Yang, S. Chen, Z. Chen, H. Qi, S. Bartling, H. Jiao, H. Junge, M. Beller, Co-tolerant heterogeneous ruthenium catalysts for efficient formic acid dehydrogenation, *Angew. Chem.* 137 (2025).
- [47] K. Köhnke, N. Wessel, J. Esteban, J. Jin, A.J. Vorholt, W. Leitner, Operando monitoring of mechanisms and deactivation of molecular catalysts, *Green Chem.* 24 (2022) 1951–1972.
- [48] K.N.M. Khalili, P. de Peinder, J. Donkers, R.J.A. Gosselink, P.C.A. Bruijninx, B.M. Weckhuysen, Monitoring molecular weight changes during technical lignin depolymerization by operando attenuated total reflectance infrared spectroscopy and chemometrics, *ChemSusChem* 14 (2021) 5517–5524.